



# New aspects on the corrosion resistance of dense refractory castables containing a novel calcium-magnesia-alumina binder

OLIVER PAWLIG\*, CHRIS PARR, JEAN-MICHEL AUVRAY, HERVÉ FRYDA, CHRISTOPH WÖHRMEYER

Kerneos SA, Paris, France

\*e-mail: oliver.pawlig@kerneos.com

---

## Abstract

This paper presents a detailed analysis and evaluation of corroded samples of  $\text{Al}_2\text{O}_3$ -pre-formed spinel and  $\text{Al}_2\text{O}_3$ -MgO castables, thus representing pre-formed spinel castables as well as *in-situ* castables. Comparisons were made between systems based upon a calcium aluminate binder and a recently developed novel calcium magnesium aluminate cement CMA 72<sup>®</sup>. A model is presented which gives an explanation for the higher corrosion resistance of the castables based upon the CMA 72<sup>®</sup> cement. The respective model is based on optical and SEM image analysis. A correlation between the thermo-mechanical properties from phase and particle distributions, microstructural features, amorphous phase of the castables and the corrosion mechanism is established. Moreover, new routes for the optimization of castable corrosion resistance via formulation control are highlighted.

**Keywords:** Corrosion resistance, Refractory castable, Calcium-magnesia-alumina binder

## NOWE ASPEKTY ODPORNOŚCI KOROZYJNEJ OGNIOTRWĄLYCH BETONÓW CIĘŻKICH OPARTYCH NA NOWYM SPOIWIE WAPNIOWO-MAGNEZJOWO-GLINOWYM

Artykuł przedstawia szczegółową analizę i ocenę skorodowanych próbek betonów ogniotrwących  $\text{Al}_2\text{O}_3$  - spinel prefabrykowany i  $\text{Al}_2\text{O}_3$ -MgO, reprezentujących betony zawierające spinel prefabrykowany i powstający *in-situ*. Dokonano porównania pomiędzy układami opartymi na cemencie glinowym i ostatnio opracowanym nowym cemencie wapniowo-spinelowym CMA 72<sup>®</sup>. Zaprezentowano model, który wyjaśnia wyższą odporność korozyjną betonów opartych na cemencie CMA 72<sup>®</sup>. Jego podstawą była analiza obrazów pochodzących z mikroskopów optycznego i skaningowego, SEM. Ustalono związek pomiędzy właściwościami termomechanicznymi kontrolowanymi przez rozkłady wielkości faz i cząstek, cechami mikrostrukturalnymi, fazą amorficzną w betonie i mechanizmem korozji. Ponadto, wskazano nowe sposoby optymalizacji odporności korozyjnej betonów poprzez kontrolę składu.

**Słowa kluczowe:** odporność na korozję, beton ogniotrwały, spoiwo wapniowo-magnezjowo-glinowe

---

## 1. Introduction

Due to their outstanding corrosion resistance to slag, castables based on alumina-spinel, alumina-magnesia, and recently, a hybrid combination of both types, have been effectively used as refractory lining in steel ladles [1-3]. With respect to slag penetration and melt-corrosion development the content of synthetic spinel or magnesita turned out to be a key parameter for the refractory material performance. It is common knowledge that the magnesium aluminate spinel content after firing should be preferably within the range of (20–40) wt.% [4]. Moreover, the size of the spinel grains is a factor of utmost importance with direct impact on the penetration resistance of the refractory [5]. More denser microstructures, less prone to slag penetration and with increased corrosion resistance result from the fine crystal sizes of the spinel grains. However, the sintering activity might be enhanced and thus, shrinkage can be induced above a certain level [6]. Upon addition of magnesita very

fine spinel can be generated which reacts with alumina fillers during firing to form *in-situ* spinel. This reaction attributes to a volume expansion [7]. If there occurs an extensive expansion, the induced stress can reach a level, resulting peeling-type crack initiation. It is common practice to counterbalance this effect by adding a small amount of microsilica to the dry mix, thereby improving the volume stability of the respective castable [3, 8]. A negative side effect from such an approach is unfortunately a reduction of castable strength at operation temperature [9]. Hence, there is the need to tailor the castable design towards a balance between expansion and sintering reactivity. In order to fulfil these requirements, a novel calcium magnesium aluminate cement (CMA<sup>®</sup>72) has been recently developed. Employing this new type of cement, the formulator can achieve the needed balance, and the refractory castable properties can be customized. Studies have been already presented, indicating that castables based on this new CMA<sup>®</sup>72 binder can better resist a large range of slag compositions [10]. The new binder is based on

a unique multiphase clinker with a microstructure of calcium aluminate phases embedded in a matrix of microcrystalline magnesium aluminate spinel crystals. This paper aims to present analyses of corroded and non-corroded samples, and to find a correlation between thermo-mechanical properties of the castables and their microstructure with focus on the mechanisms that underlie the corrosion of castables.

## 2. Materials and test methods

The chemical and mineralogical composition of calcium aluminate cement (CAC) and CMA<sup>®</sup>72 was determined employing XRF and XRD, respectively. The results are shown in Table 1.

Table 1. Chemical and mineralogical compositions in wt. %.

Chemistry	Al <sub>2</sub> O <sub>3</sub>	CaO	MgO	SiO <sub>2</sub>
Secar <sup>®</sup> 71	68.7-70.5	28.5-30.5	<0.5	0.2-0.6
CMA <sup>®</sup> 72	69-71	8-11	16-22	<1.0
Mineralogy	CA	CA <sub>2</sub>	MA	C <sub>2</sub> AS
Secar <sup>®</sup> 71	56-61	39-44	0	<1
CMA <sup>®</sup> 72	18-22	8-12	68-72	<1

Both cements have a Blaine specific surface area close to 4000 cm<sup>2</sup>/g with a median  $d_{50}$  of 15-18 μm, measured with a laser granulometer. In Table 2 the compositions of model castables used in this study are presented. The formulations

Table 2. Composition of alumina-spinel (MA) and alumina-magnesia (M) model castables in wt. % and estimation of their chemical compositions (MA content for M1 and M2 after firing at 1550 °C).

Castable	MA1	MA2	M1	M2
Binder System	CAC	CMA	CAC	CMA
Tabular Alumina 0-6 mm	60	61	75.5	70
Reactive Alumina	11	11	11	8
Sintered Spinel 0-1 mm	13	10		
Sintered Spinel < 90 μm	10			
Sintered MgO < 74 μm			6.5	3
CAC (Secar <sup>®</sup> 71)	6		6	
CMA (CMA <sup>®</sup> 72)		18		18
Silica (Elkem Microsilica <sup>®</sup> 971U)			1	1
PCE (Peramin <sup>®</sup> AL 200)	+0.1	+0.1	+0.15	+0.1
Water	+4	+4	+4.5	+4.5
MA	23	23	23	23
CaO	1.7	1.7	1.7	1.7
MgO total	5.2	5.8	6.5	6.6
Al <sub>2</sub> O <sub>3</sub>	93.1	92.4	90.8	90.6
SiO <sub>2</sub>			1.0	1.0
TOTAL	100	100	100	100

Table 3. BOF slag composition (slag B).

[wt.%]	Al <sub>2</sub> O <sub>3</sub>	SiO <sub>2</sub>	FeO	MnO	CaO	MgO	C/S
Slag B	2	15	19	6	53	5	3.5

MA1 and MA2 contain pre-reacted sintered spinel whereas M1 and M2 are designed with free MgO (Periclase). M2 is a hybrid system since it contains MgO as well as MA spinel brought in about by the CMA<sup>®</sup>72 binder. The formulation logic here is to maintain the chemical composition of the castable and the same total MA phase after sintering. The total amount of binder has been chosen to ensure that these castables are low cement castables (LCC) with a constant CaO content of 1.7 wt.% as indicated in Table 2. A polycarboxylate ether based additive, Peramin<sup>®</sup> AL200, was chosen to efficiently deflocculate the castables at very low amounts of mixing water.

Corrosion and penetration tests were performed according to ASTM C874-99, employing a laboratory scale rotary kiln. The test slag was a BOF slag with a composition as shown in Table 3. The slag resistance and additional properties measured at high temperature have been already presented [10]. Microstructure analyses were done with a scanning electron microscope (SEM) using backscattered images on polished surfaces. The chemical compositions of the phases have been studied using energy dispersive spectroscopy (EDS). Specimen for sample preparation were pre-fired for 5 h at 1550 °C. Subsequently, the specimen was exposed to an iron rich slag in the laboratory kiln at 1550 °C.

## 3. Results and discussion

### 3.1. Microstructural analyses of non-corroded castables

SEM images of non-corroded samples are shown in Fig. 1. The microstructure of alumina-spinel castable with CAC (Fig. 1a) is represented by a porous matrix embedding tabular alumina (TA) and spinel (MA) aggregates. Moreover, interlocking CA<sub>6</sub> and fine spinel grains were found. Large quantities of porous clusters of CA<sub>6</sub> needles are at the edge of TA aggregates and in the castable's matrix. They were also found at the border of MA grains. The CA<sub>6</sub> needles have a length of 10-20 μm and thickness in the range of 0.5-1.0 μm.

In Fig. 1b the microstructure of the same castable, however formulated with CMA<sup>®</sup>72, is shown. Peculiarities here are uniformly distributed very fine spinel grains and needles of CA<sub>6</sub> almost as if sintered together into a dense matrix. Compared to the MA1 castable the respective CA<sub>6</sub> needles exhibit a lower length/thickness ratio. In addition, there is a strong interlocking between TA, MA and the matrix. Fig. 1c shows the microstructure of alumina magnesia castable with CAC. Here, the CA<sub>6</sub> phase can be found primarily at the boundaries of TA aggregates. The crystals have a platy morphology. Due to the lack of available alumina used for the generation of *in-situ* spinel, there is a shortage of CA<sub>6</sub> phase in the matrix. However, in a more dense microstructure of alumina-magnesia castable formulated with CMA<sup>®</sup>72 (Fig. 1d), a different CA<sub>6</sub> phase location and morphology is observed. The bonding matrix between TA aggregates is mainly constituted of acicular CA<sub>6</sub> crystals at the TA boundaries while coupled crystalline CA<sub>6</sub> platelets are homogeneously distributed throughout the microstructure and bridging fine spinel particles from CMA<sup>®</sup>72 and from *in-situ* formation. Furthermore, the fine spinel particles remain well distinguished from other constituents of the matrix. The

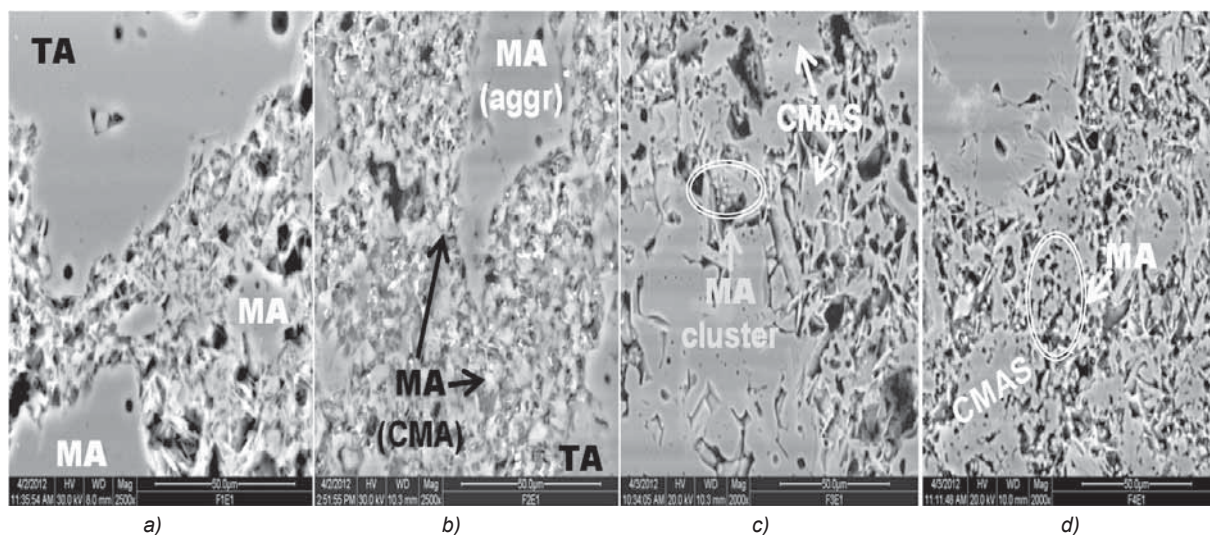
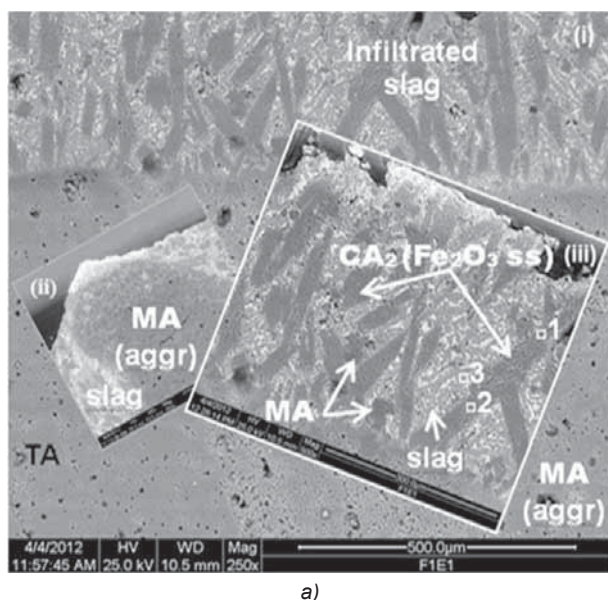
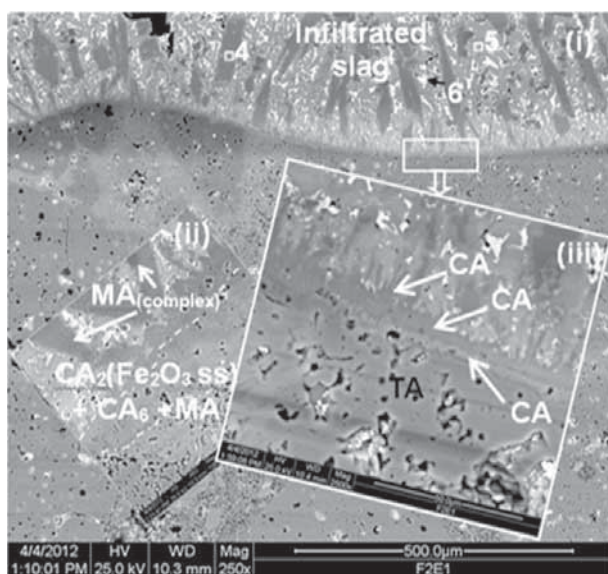


Fig. 1. SEM images of non-corroded alumina-spinel castables (MA) and alumina-magnesia castables (M) after firing at 1550 °C: a) MA1 (CAC), b) MA2 (CMA®72), c) M1 (CAC), d) M2 (CMA®72).



a)



b)

Fig. 2. SEM images of the corroded alumina-spinel castables: a) – MA1 (CAC) and b) – MA2 (CMA®72).

addition of polycarboxylate ether based additive has probably contributed to a greater amount of coupled  $CA_6$  platelets in both alumina-magnesia castables. The detected variety in  $CA_6$  morphology and distribution suggests possibilities of mastering reaction routes to tailor their shape and growth.

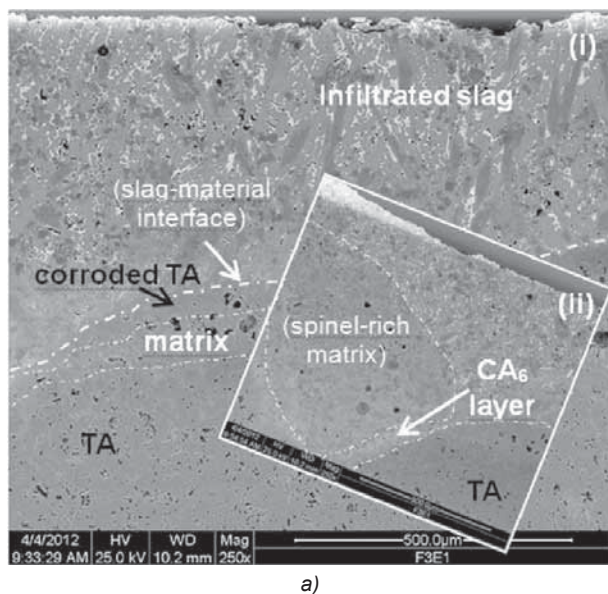
### 3.2. Microstructural analyses of corroded castables

SEM images of the microstructures, resulting from alumina-spinel castables formulated with CAC and CMA®72 after corrosion tests, are shown in Fig. 2. An altered layer with a thickness of approx. 500  $\mu\text{m}$ , as a result of the slag penetration into the MA1 castable, can be seen in Fig. 2a. The progressive degradation of the refractory material and continuous infiltration as well as diffusion of the slag led to the phase transformation and the formation of new calcium aluminate based multi-oxide phase assemblages containing some slag elements, such as Fe, Mn and Si. In particular, a solid phase zone with an elongated shape in silica-lime rich liquid is the most noticeable. EDS analyses revealed a variety of compositions derived from  $CA_2$  within the elongated zones (points 1 and 2, Table 4).

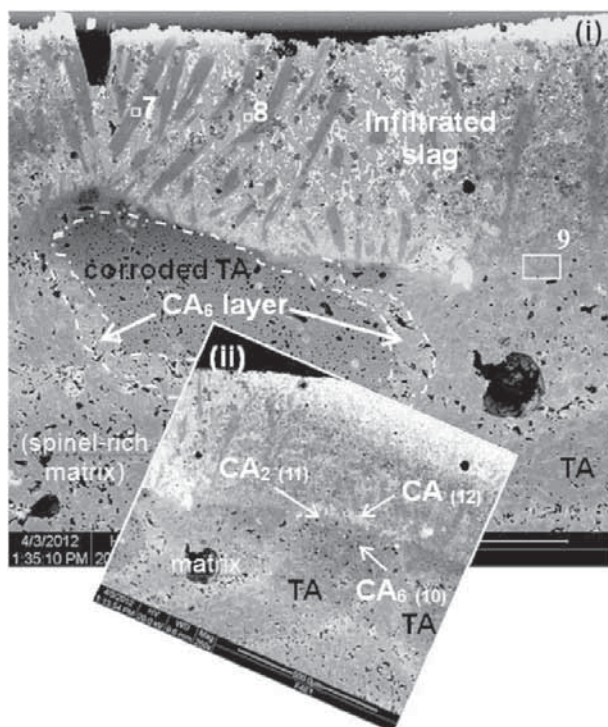
Furthermore, some fine spinel grains from the matrix randomly distributed throughout the altered layer after the slag attack, are also visible (Fig. 2a (iii)). An example of interaction between a coarse spinel aggregate and slag is given in Fig. 2a (ii). Here, slag penetration occurs along matrix grain boundaries and via the interconnected porosity, indicating that there is an interaction between slag and castable. This interaction exhibits the typical pattern of a dissolution-precipitation mechanism with progressive dissolution of alumina and spinel, followed by precipitation of new calcium aluminate phases enriched in silica and iron from the reaction with calcium from the slag. In MA2 (CMA®72), there is a clear interface between the altered layer and the refractory with a thickness of approx. 400  $\mu\text{m}$  (Fig. 2 b (i)). The penetration of the slag and its interaction with the castable resulted in the formation of calcium-aluminate-ferrite crystals elongated in shape and with a stoichiometry derived from  $CA_2$  (point 4). The surrounding glassy phase (point 5) contains less iron

Table 4. EDS analyses (wt.%) of the corroded castables.

	1	2	3	4	5	6	7	8	9	10	11	12
O	46.6	46.9	44.3	48.9	46.0	41.7	46.8	43.1	48.2	49.2	46.3	44.1
Mg	6.7	0	0	0	0	0	0	0	10.1	0.3	0	0
Al	32.1	35.1	17.2	34.8	18.9	11.5	36.5	17.0	33.1	44.4	38.3	21.8
Ca	6.5	14.7	25.1	13.5	25.1	25.4	14.4	25.2	5.6	5.7	14.3	25.1
Si	0.7	0.6	7.1	0.3	6.7	1.3	0	6.4	0.3	0.4	0	5.9
Mn	2.2	0.3	0.6	0	0	4.4	0	1.2	0.65	0	0	0
Fe	5.2	2.4	5.7	2.5	3.3	15.7	2.3	7.1	2.05	0	1.1	3.1



a)



b)

Fig. 3. SEM images of the corroded alumina-magnesia castables: (a) M1 (CAC) and (b) M2 (CMA<sup>®</sup>72).

than MA1 castable. In higher magnification (Fig. 2b (ii)) these elongated crystals appear to act as a barrier against the further slag penetration. The interface between the slag and a TA aggregate consists of 3 mono-mineral layers derived from CA<sub>6</sub>, CA<sub>2</sub> and CA successively (Fig. 2b (iii)). Therefore, a change in the chemical composition and/or viscosity of molten slag resulting from more homogeneous distribution of fine spinel particles and consequently, higher absorption of the metallic cations, such as Fe<sup>2+</sup>, Fe<sup>3+</sup> and Mn<sup>2+</sup>, contribute to the higher corrosion resistance of CMA<sup>®</sup>72 based castable.

Fig. 3 shows microstructures of alumina-magnesia castables after the corrosion test. It can be clearly seen that the slag-refractory interfaces are not well pronounced. The altered layer of M1 castable has a thickness of approx. 500 μm (Fig. 3a (i)) while the layer of M2 castable with CMA<sup>®</sup>72 has a thickness of about 380 μm (Fig. 3b (i)). A strong interlocking network between CA<sub>6</sub> and microcrystalline spinel grains, associated to a denser microstructure, limits a further infiltration of the slag (point 9).

#### 4. Conclusions

The microstructural features of non-corroded and corroded alumina-spinel and alumina-magnesia castables after a rotary furnace test have been studied. The CMA<sup>®</sup>72 based castables exhibit higher corrosion resistance and lower slag penetration. The root causes behind that finding are the following:

- The slag penetrates into the castable by partially dissolving alumina from TA aggregates and CA<sub>6</sub> from the matrix.
- Calcium aluminate phases incorporating slag constituents (Fe, Si) are formed inside a CaO-rich layer.
- Microcrystalline and homogeneously distributed spinel is more resistant to a progressive slag attack by uptake of Fe and Mn, thus changing the viscosity and the composition of the liquid phase inside the altered layer.
- The slag/refractory interface consists of a succession of mono-mineral layers. The TA aggregates are surrounded by a CA<sub>6</sub> layer which reveals to be a diffusion barrier.

#### References

- [1] Dott, K.H.: Monolithic ladle lining at SSAB Tunnpått in Luleå, Sweden, *RHI Bulletin*, 1, (2008), 34-37.
- [2] Yamamura, T.: Development of alumina-spinel castables for steel ladles, *Taikabutsu*, 42, 8, (1990), 427-434.

- [3] Naaby, H., Abbildgaard, O., Stallmann, G., Wöhrmeyer, C., Meidell, J.: Refractory wear mechanisms and influence on metallurgy, in *Proc. 37<sup>th</sup> Int. Colloquium on Refractories*, Aachen, Germany, (1994), 198-204
- [4] Kanatani, T., Imaiida, Y.: Application of an alumina-spinel castable to the teeming ladle for stainless steelmaking, in *Proc. UNITECR'93*, (1993), 1255-1266.
- [5] Nakashima, M., Isobe, T., Itose, S.: Improvement in corrosion of alumina-spinel castable by adding ultrafine spinel powder, *Taikabutsu*, 52, 2, (2000), 65-72.
- [6] Bhatnagar, V., Mukhopadhyay, S., Natarajan, C.: Development of improved quality spinel castable for steel ladle bottom, *Proc. UNITECR'05*, (2005), 162-166.
- [7] Braulio, M. A. L., Milanez, D. H., Sako, E. Y., Bittencourt, L. R. M., Pandolfelli, V. C.: Expansion behaviour of cement bonded alumina-magnesia refractory castables, *Am. Ceram. Soc. Bull.*, 86, 12, (2007), 9201-9206.
- [8] Bier, T., Parr, C., Revais, C., Vialle, M.: Spinel forming castables: Physical and chemical mechanisms during drying, *Refractories Application*, 4, (2000), 3-4.
- [9] Ko, Y.C.: Development and production of  $Al_2O_3$ -MgO and  $Al_2O_3$ -spinel castables for steel ladles, *Mining and Metallurgy (Taipei)*, 47, 1, 132-140.
- [10] Wöhrmeyer, C., Parr, C., Fryda, H., Auvray, J. M., Touzo, B., Guichard, S.: New spinel containing calcium aluminate cement for corrosion resistant castables, *Proc. UNITECR'11*, (2011), 1255-1266.



---

*Received 29 April 2013, accepted 3 September 2013*